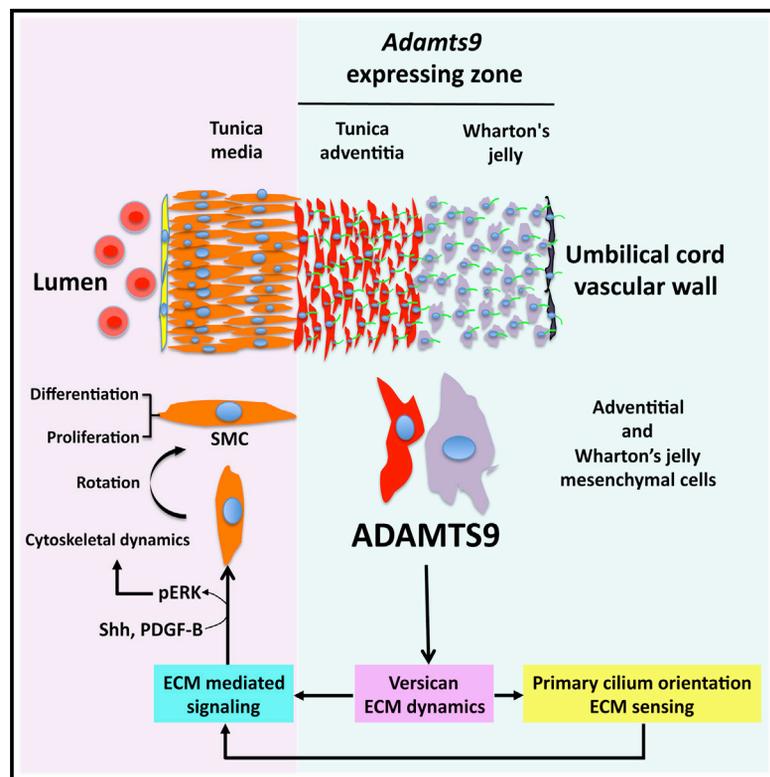# Cell Reports

ADAMTS9-Mediated Extracellular Matrix Dynamics Regulates Umbilical Cord Vascular Smooth Muscle Differentiation and Rotation

Graphical Abstract

Authors

Sumeda Nandadasa, Courtney M. Nelson, Suneel S. Apte

Correspondence

aptes@ccf.org

In Brief

Nandadasa et al. show that ADAMTS9, a secreted metalloprotease, is essential for versican proteolysis during mouse umbilical cord vascular development. In an *Adamts9* gene trap mutant, they report non-autonomous impairment of crucial steps in smooth muscle signaling pathways and differentiation that are essential for construction of the umbilical vessel wall.

Highlights

- Cell-membrane ADAMTS9 suffices for gastrulation, but not for later mouse development

- ADAMTS9 is required for versican proteolysis during umbilical cord vascular growth

- Extracellular matrix accumulation impairs umbilical smooth muscle differentiation

- Matrix dynamics regulates primary cilium orientation and Shh and PDGFRβ signaling

CellPress

OPEN
ACCESS

Cell Reports

Report

ADAMTS9-Mediated Extracellular Matrix Dynamics Regulates Umbilical Cord Vascular Smooth Muscle Differentiation and Rotation

Sumeda Nandadasa,[1] Courtney M. Nelson,[1] and Suneel S. Apte[1,*]
[1]Department of Biomedical Engineering, Cleveland Clinic Lerner Research Institute, Cleveland, OH 44195, USA
*Correspondence: aptes@ccf.org
http://dx.doi.org/10.1016/j.celrep.2015.05.005

SUMMARY

Despite the significance for fetal nourishment in mammals, mechanisms of umbilical cord vascular growth remain poorly understood. Here, the secreted metalloprotease ADAMTS9 is shown to be necessary for murine umbilical cord vascular development. Restricting it to the cell surface using a gene trap allele, $Adamts9^{Gt}$, impaired umbilical vessel elongation and radial growth via reduced versican proteolysis and accumulation of extracellular matrix (ECM). Both $Adamts9^{Gt}$ and conditional $Adamts9$ deletion revealed that ADAMTS9 produced by mesenchymal cells acted non-autonomously to regulate smooth muscle cell (SMC) proliferation, differentiation, and orthogonal reorientation during growth of the umbilical vasculature. In $Adamts9^{Gt/Gt}$, we observed interference with PDGFRβ signaling via the mitogen-activated protein kinase/extracellular signal-regulated kinase (MAPK/ERK) pathway, which regulates cytoskeletal dynamics during SMC rotation. In addition, we observed disrupted Shh signaling and perturbed orientation of the mesenchymal primary cilium. Thus, ECM dynamics is a major influence on umbilical vascular SMC fate, with ADAMTS9 acting as its principal mediator.

INTRODUCTION

The umbilical cord is the sole fetal-maternal link in placental mammals, conducting blood from the fetus for exchange in the placenta. Excessively long or short cords or cord vascular anomalies are associated with high fetal morbidity and a risk of stillbirth (Benirschke et al., 2012). Umbilical vessels must remodel extensively after chorio-allantoic fusion, as they grow to accommodate increasing fetal metabolic demand. However, this process has not been studied, and little is known about umbilical cord extracellular matrix (ECM) remodeling.

ECM comprises networks of collagenous and non-collagenous proteins (Mouw et al., 2014) and is remodeled in all morphogenetic processes, e.g., branching morphogenesis, and sculpting

of interdigital webs and heart valves (Bonnans et al., 2014; Dupuis et al., 2011; McCulloch et al., 2009). A pre-gastrulation embryo has a sparse, cell-associated ECM (Kwon et al., 2008; Miner et al., 2004). Later, interstitial ECM expands in mesenchyme, but it is a provisional ECM containing fibronectin (Peters and Hynes, 1996), hyaluronan (Camenisch et al., 2000), and the hyaluronan-binding proteoglycan versican (Naso et al., 1995) and less of mature ECM components such as collagens and elastin. Provisional ECM provides a foothold for cell attachment and is easily remodeled. It gradually transitions to a specialized matrix toward birth, although the umbilical cord, which is not destined for a post-natal life, maintains a proteoglycan-rich matrix named Wharton's jelly (Sobolewski et al., 1997), containing one to two arteries and a vein, the whole sheathed in mesothelium.

ADAMTS (A disintegrin-like and metalloprotease with thrombospondin type 1 motifs) proteinases (Apte, 2009) remodel provisional ECM in diverse morphogenetic processes (Dupuis et al., 2011; Enomoto et al., 2010; McCulloch et al., 2009; Stankunas et al., 2008; Stupka et al., 2013). ADAMTS9 is highly conserved; its *C. elegans* ortholog, Gon-1, is required for gonadal morphogenesis (Blelloch et al., 1999), and the *D. melanogaster* ortholog AdamTS-A is essential for salivary gland morphogenesis and germ cell migration (Ismat et al., 2013). *Adamts9* null mice die at the onset of gastrulation (Enomoto et al., 2010), but haploinsufficient and conditionally targeted mice identified later developmental roles (Dubail et al., 2014; Enomoto et al., 2010; Kern et al., 2010). Here, an *Adamts9* gene-trap mutant, where ADAMTS9 is restricted to the cell surface, revealed distinct pools of ADAMTS9 activity, cell proximal and distal, and requirement of the distal pool for umbilical cord vascular development in mice. ADAMTS9 is thus identified as a crucial component of the pathway connecting ECM dynamics to cellular regulation in this context.

RESULTS AND DISCUSSION

An *Adamts9* Gene Trap Generates Membrane-Anchored ADAMTS9

The $Adamts9^{Gt}$ mouse allele was made from embryonic stem (ES) cells with UPATrap insertion in intron 30 (Figure S1A). $Adamts9^{Gt/+}$ mice were externally normal and fertile. Tiled PCR of $Adamts9^{Gt/+}$ genomic DNA identified the UPATrap insertion
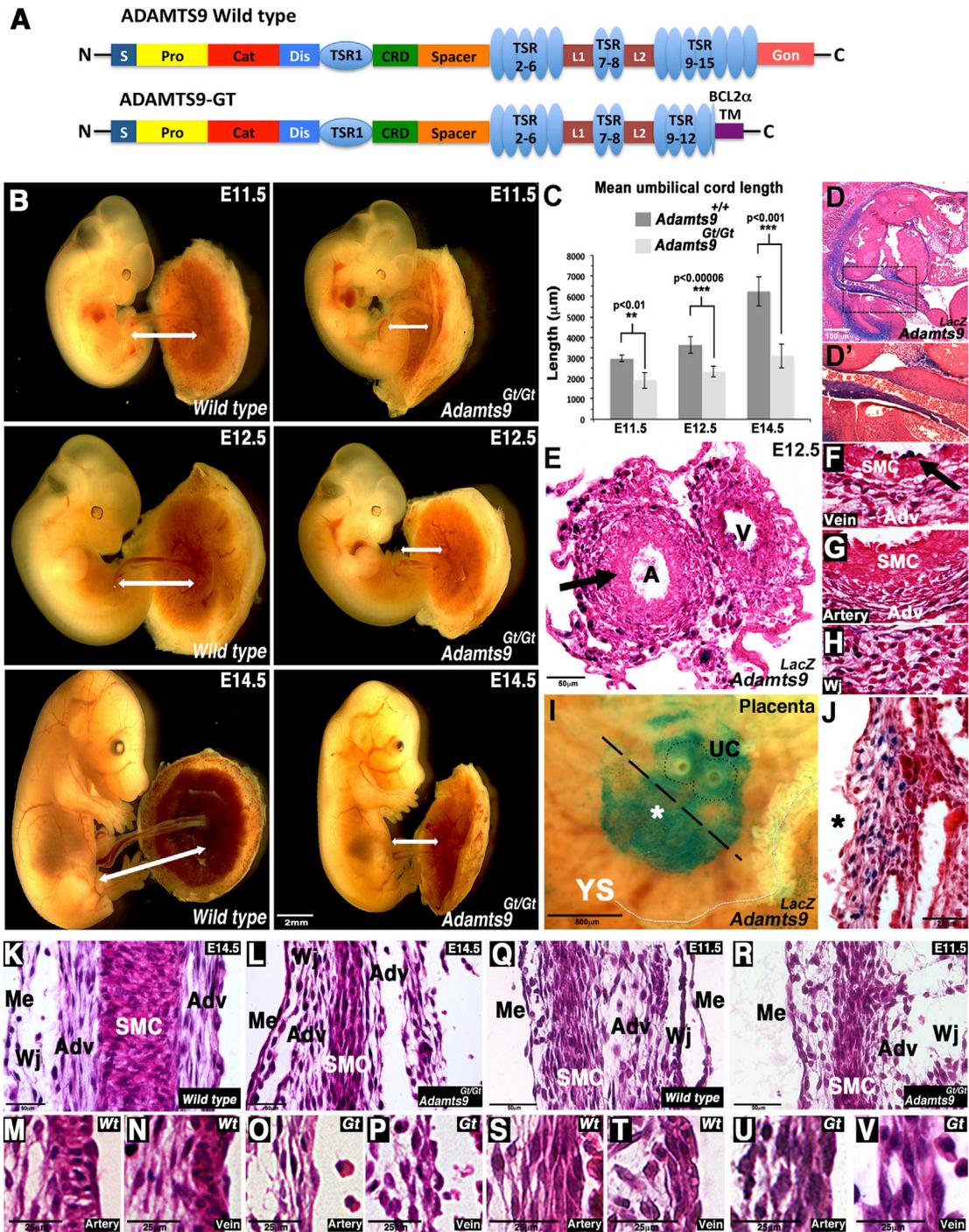
Figure 1. An *Adamts9* Gene Trap Impairs Umbilical Cord Development

(A) Schematic of WT ADAMTS9 and ADAMTS9-GT. S, signal peptide; Pro, propeptide; Cat, catalytic domain; Dis, Disintegrin-like module; CRD, cysteine rich module; L1–L2, linkers 1–2; TM, Transmembrane domain.

(B) *Adamts9^Gt/Gt* embryos have short umbilical cords (arrows).

(C) WT, but not *Adamts9^Gt/Gt*, umbilical cords double in length between E11.5 and E14.5 (n = 7 cords for each group at E12.5, n = 3 cords for each group at E11.5 and E14.5. Error bars represent SD; p values are determined by Student's t test).

(D and D') β-gal and eosin staining of E12.5 *Adamts9^LacZ/+* embryo showing *Adamts9* expression (blue) at the embryo umbilical cord insertion site.

(E–H) Cross-sections of E12.5 *Adamts9^LacZ/+* umbilical cord showing *Adamts9* expression (blue) in adventitia, Wharton's jelly, and venous endothelium. Arrow in (E) indicates the tunica media. (F)–(H) show higher magnification of the umbilical vein, artery, and Wharton's jelly. Black arrow in (F) shows *Adamts9* expression in the venous endothelium.

(legend continued on next page)

site (Figure S1B), allowing genotyping of *Adamts9*[Gt] and WT alleles (Figure S1C).

In *Adamts9*[Gt], splicing of exon 30 to the Bcl2α splice acceptor from UPATrap led to a frame-shift in thrombospondin type 1 repeat (TSR) 13, deleted three downstream TSRs and the Gon-1 domain and resulted in a stop codon 44 amino acids downstream (Figures 1A and S1D). The new C terminus, DAFVELYGPSMRPLFDFSWLSLK TLLSLALVGACITLGAYLSHK, matched the C terminus of human Bcl2α, a mitochondrial membrane protein (transmembrane domain underlined). Thus, *Adamts9*[Gt] expressed a C-terminally truncated, constitutively membrane-anchored ADAMTS9 (Figure 1A). Despite this, *Adamts9*[Gt/Gt] embryos underwent gastrulation and were externally normal until E11.5 (Figure 1B; Table S1).

Expression plasmids for ADAMTS9-GTa and ADAMTS9-GTb, reflecting splice variants affecting TSR11 and TSR12 (GenBank: XM_006505260.1, XM_006505263.1) (Figures S1E and S1F), and a control construct (ADAMTS9 N-TSR12) were generated (Figure S2A). We observed localization of ADAMTS9-GTa/b to the secretory pathway and cell membrane (Figure S2B) but not to mitochondria in transfected COS-1 cells (Figure S2B). Western blotting consistently showed less cellular ADAMTS9-GT than the control construct in transfected cells, and ADAMTS9-GTa/b were undetectable in the medium (Figure S2C). Cell-surface biotinylation demonstrated ADAMTS9 N-TSR12 zymogen and a smaller, furin-processed (mature) form (Figure S2D), which disappeared along with reduction of biotinylated zymogen upon trypsinization, consistent with work showing that ADAMTS9 zymogen bound avidly to the cell surface, but the mature form did not (Koo et al., 2006, 2007). ADAMTS9-GTa/b were biotinylated and sensitive to trypsin, confirming cell-surface location, but only ADAMTS9-GTa/b zymogen was detected, suggesting a lack of furin processing (Figure S2D). Thus, ADAMTS9-GT was present at lower levels in transfected cells than WT ADAMTS9, restricted to the cell surface, and not processed to maturity. ADAMTS9-GT zymogen is likely to be proteolytically active (Koo et al., 2007), but its cell-surface confinement and reduced cellular levels implied compromised function.

Adamts9[Gt] Is a Hypomorphic Allele

Adamts9[Gt/+] mice lacked a highly penetrant ocular anomaly identified in *Adamts9*[lacZ/+] mice (Koo et al., 2010), and *Adamts9*[Gt/Gt] mice, unlike *Adamts9*[LacZ/LacZ] and *Adamts9*[Del/Del] mice, survived past gastrulation (E7.0). ADAMTS20, which has an identical domain structure as ADAMTS9, was previously shown to work cooperatively with it in palatogenesis and skin pigmentation (Enomoto et al., 2010; Silver et al., 2008). We

introduced an *Adamts9*[Gt] allele into *Adamts20*[Bt/Bt], a mutant with white spotting in the lumbar region (Rao et al., 2003) (Figure S3A). Like *Adamts9*[LacZ/+]; *Adamts20*[Bt/Bt] or *Adamts9*[Del/+]; *Adamts20*[Bt/Bt] mice, these mice died at birth with cleft palate (Dubail et al., 2014; Enomoto et al., 2010) and lacked skin melanoblasts (Silver et al., 2008) (Figures S3A–S3F). Thus, *Adamts9*[Gt] is a hypomorphic allele functionally equivalent to an *Adamts9* null allele in genetic interactions with *Adamts20*[Bt].

Adamts9[Gt/Gt] Embryos Have Impaired Umbilical Cord Growth

Adamts9[Gt/+] intercrosses did not provide *Adamts9*[Gt/Gt] mice at birth or weaning (Table S1). A Mendelian proportion of *Adamts9*[Gt/Gt] embryos was obtained from E12.5–E14.5, but none survived past E15.5. *Adamts9*[Gt/Gt] embryos older than E11.5 had unusual proximity to the placenta, revealing short umbilical cords with minimal growth beyond from E11.5–E14.5, whereas the WT cords doubled their length over this period (Figures 1B and 1C). Coupled with minimally reduced embryo and placenta weight (Figures 1B and S3G), this implied loss of a specific function in the umbilical cord with intrauterine embryonic growth restriction (IUGR) as a sequel. Although placental size was comparable (Figure 1B), the endothelium-lined fetal compartment of *Adamts9*[Gt/Gt] placenta consistently contained stacks of nucleated red blood cells after E12.5 (Figures S3H–S3I'), suggesting impaired umbilical cord circulation and secondary IUGR of *Adamts9*[Gt/Gt] embryos after E11.5. E8.5 to E12.5 *Adamts9*[LacZ/+] conceptuses were obtained by crossing WT females with *Adamts9*[LacZ/+] males to bypass β-gal staining arising in maternal tissues. *Adamts9* was expressed in the umbilical cord insertion sites in the embryo (Figures 1D and 1D'), and placenta (Figures 1I and 1J) comprising Wharton's jelly transition zones. β-gal staining was strongest in the adventitia of the umbilical vessels, Wharton's jelly mesenchyme, and endothelial cells of the umbilical vein but not arteries, whereas vascular smooth muscle cells (VSMCs) were unstained (Figures 1E–1H). An ADAMTS9 antibody is presently unavailable to investigate protein distribution.

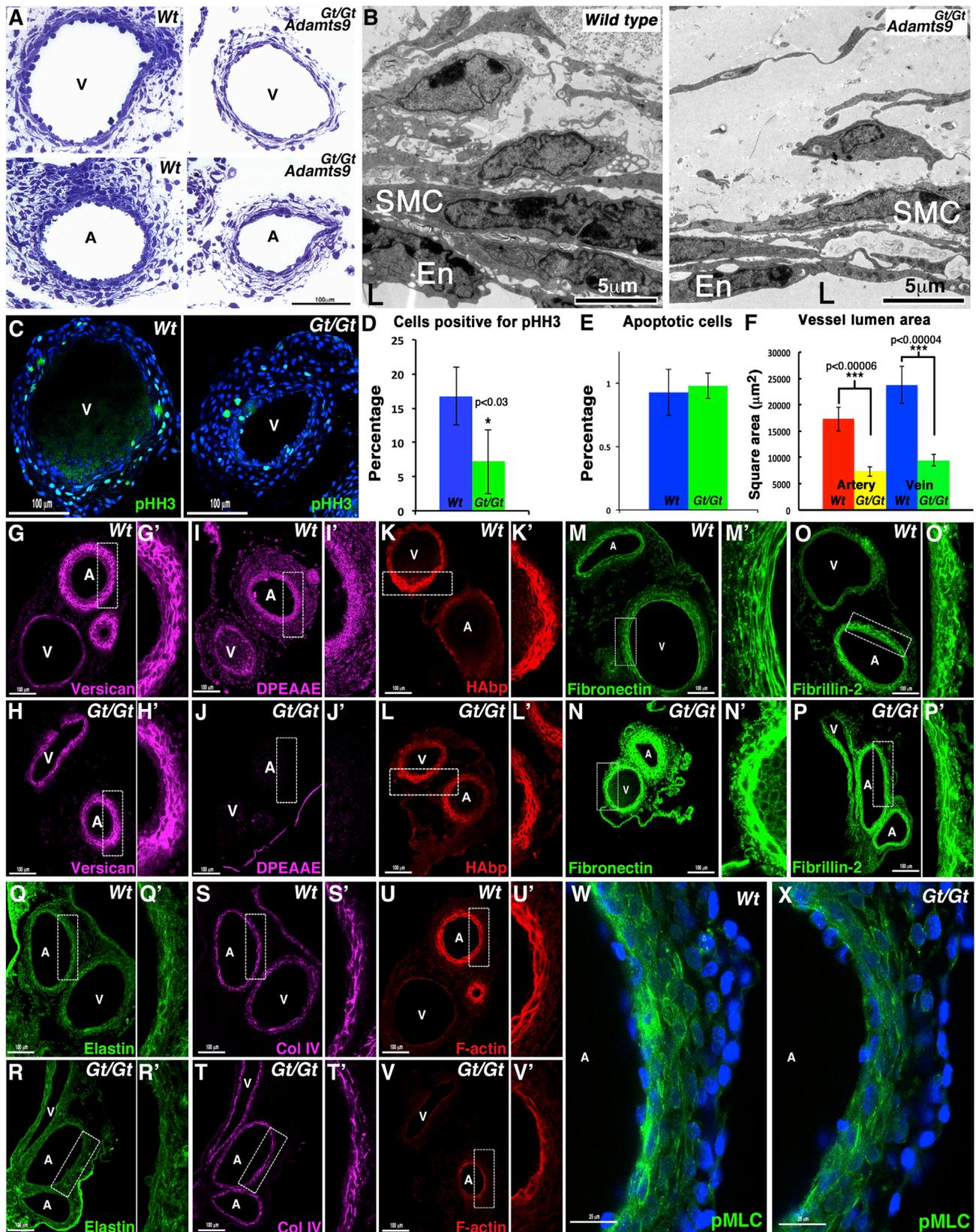### VSMC Orthogonal Orientation Is Impaired in *Adamts9*[Gt/Gt] Umbilical Cords

By E14.5, WT umbilical cord mesenchyme formed two distinct layers around each artery (Figure 1K), namely a 6- to 12-cells-thick zone of longitudinally oriented tunica adventitia cells and an outer zone of randomly oriented and sparse mesenchymal cells (Wharton's jelly mesenchyme). In E14.5 WT arterial and venous walls, VSMCs were oriented orthogonally to adventitial cells, i.e., circumferentially with respect to the lumen (Figures

(I and J) En face view of E12.5 *Adamts9*[LacZ/+] placenta shows β-gal staining at the umbilical cord insertion site. The dotted line circles umbilical vessels. Dashed line indicates the section plane in (J), showing that *Adamts9* expression is confined to Wharton's jelly at the umbilical cord insertion site.

(K–P) H&E-stained sagittal sections of E14.5 WT (K, M, and N) and *Adamts9*[Gt/Gt] (L, O, and P) umbilical cords. In (K) and (L), sections are tangential through the tunica media of the umbilical artery. In (M)–(P), sections are taken through the lumina. WT SMCs are aligned orthogonal to adventitial cells and the endothelium, but *Adamts9*[Gt/Gt] SMCs are fewer and co-aligned with adventitial cells.

(Q–V) At E11.5, both WT (Q, S, and T) and *Adamts9*[Gt/Gt] (R, U, and V) VSMCs are co-aligned with adventitial cells. (Q) and (R) show tangential sections through the tunica media of the umbilical artery; (S)–(V) are through the lumina.

Scale bars represent 2 mm in (B); 100 μm in (D); 50 μm in (E); 500 μm in (I); 25 μm in (J); 50 μm in (K)–(L), (Q), and (R); and 25 μm in (M)–(P) and (S)–(V). Me, mesothelium; Wj, Wharton's jelly; Adv, adventitia. See also Figures S1–S3 and S5 and Table S1.

(legend on next page)

1K, 1M, and 1N). Strikingly, VSMCs of E14.5 $Adamts9^{Gt/Gt}$ umbilical vessels were co-aligned with adventitial cells (Figures 1L, 1O, and 1P). By E14.5, both the VSMCs and adventitia of the mutant umbilical vessels were less densely populated than WT umbilical vessels (Figures 1L, 1O, and 1P).

At E11.5, the $Adamts9^{Gt/Gt}$ umbilical vessel walls resembled the WT (Figures 1Q and 1R); i.e., umbilical arteries comprised one to two layers of co-aligned VSMCs and adventitial cells. Thus, WT VSMCs, which are longitudinally oriented at E11.5, re-orient orthogonally by E14.5 (Figures 1K and 1Q), as previously observed in the pulmonary artery (Greif et al., 2012). In contrast, $Adamts9^{Gt/Gt}$ VSMCs fail to undergo reorientation (Figures 1L and 1R).

Loss of ADAMTS9 Function Alters ECM Dynamics and Reduces VSMC Proliferation

After E12.5, when umbilical vessel growth accelerates, $Adamts9^{Gt/Gt}$ umbilical vessels had fewer VSMC layers and narrower lumina, indicating impaired radial expansion (Figures 2A and 2F). We observed reduced cellularity and increased intercellular spacing of VSMC and Wharton's jelly cells in $Adamts9^{Gt/Gt}$ umbilical cords (Figure 2A). Transmission electron microscopy (TEM) identified overabundant amorphous, non-fibrillar interstitial ECM (Figure 2B), although collagen fibril morphology was unaltered and $Adamts9^{Gt/Gt}$ umbilical cord VSMC had abundant organelles (Figures S4A and S4B). Phospho-histone H3 (pHH3) staining showed fewer proliferating cells in mutant umbilical vessels (Figures 2C, 2D, S4C, and S4D) and cleaved caspase-3 staining revealed minimal cell death in both WT and mutant umbilical cords (Figures 2E, S4E, and S4F).

Versican, an ADAMTS9 substrate, forms aggregates with hyaluronan in Wharton's jelly (Gogiel et al., 2003). A polyclonal antibody against the versican GAG-β domain (present in splice isoforms V0 and V1) detected versican in the umbilical vascular wall and Wharton's jelly (Figures 2G and 2H). Versican proteolysis (detected by a neo-epitope antibody to-DPEAAE[441]) (Sandy et al., 2001) was detectable in WT umbilical cords but not in $Adamts9^{Gt/Gt}$ mutants (Figures 2I and 2J). In the WT placenta, versican and DPEAAE staining coincided with

$Adamts9$ expression, and there was less cleaved versican in the $Adamts9^{Gt/Gt}$ mutant (Figures S4H–S4K). Endomucin labeled the labyrinth vessels, which were morphologically similar between WT and mutant placentas (Figures S4H–S4K). Hyaluronan-binding protein (HAbp) staining of umbilical cords was unaltered (Figures 2K and 2L), but fibronectin and fibrillin-2, typical provisional matrix constituents, showed enhanced staining in $Adamts9^{Gt/Gt}$ umbilical vessels (Figures 2M–2P'). Elastin is normally present in a non-laminar pattern surrounding individual VSMCs in the embryonic mouse aorta (Wagenseil and Mecham, 2009), similar to its distribution in WT umbilical cord SMCs at E12.5, and was decreased in the mutant vessels (Figures 2Q–2R'), but collagen IV staining was comparable (Figures 2S–2T'). The filamentous actin (F-actin) network and F-actin-interacting contractile proteins drive cell shape changes during morphogenesis (Nandadasa et al., 2009). Phalloidin and phosphorylated myosin light chain (pMLC) staining indicating the F-actin network and contractility competence, respectively, were greatly reduced in $Adamts9^{Gt/Gt}$ VSMCs (Figures 2U–2X). αSMA immunofluorescence revealed significantly lower staining intensity in mutant VSMCs (Figures 3A and 3B). Collectively, these findings point to severe impairment of $Adamts9^{Gt/Gt}$ VSMC differentiation.

Altered ECM Dynamics Attenuates Shh and PDGFR-β Signaling in the Umbilical Vascular Wall

Shh signaling is critical for VSMC differentiation in the dorsal aorta and is required for investment by multiple VSMC layers (Passman et al., 2008). Strong expression of Shh, Patched-1, and Gli-1 was previously seen in the umbilical cord at E13.5 but not at E11.5 (Haraguchi et al., 2007). In $del5$-LacZ mice, which report Hh signaling, β-gal staining in the umbilical cord was observed from E12.0 (Haraguchi et al., 2007). We observed strong Shh staining in the tunica media of E12.5 WT but not mutant umbilical vessels (Figures 3C–3D'). Gli-1, a reporter of Shh signaling activity, and Sca-1, a marker of the progenitor state maintained by Shh signaling (Passman et al., 2008), were reduced in $Adamts9^{Gt/Gt}$ umbilical vessels (Figures 3E–3H). The PDGFR-β signaling pathway is critical for recruitment of VSMC and pericytes by endothelial cells (Armulik et al., 2011), and

Figure 2. ADAMTS9 Is Required for Umbilical Cord VSMC Growth and ECM Homeostasis

(A) Toluidine blue staining of E12.5 WT and $Adamts9^{Gt/Gt}$ umbilical cords shows smaller, thinner walled vessels in the mutant.

(B) TEM of WT and $Adamts9^{Gt/Gt}$ umbilical vein shows increased amorphous ECM in the mutant.

(C and D) pHH3 staining in umbilical vein shows reduced cell proliferation in the mutant (n = 4 cords for each group. Error bars represent SD; p values are determined by Student's t test).

(E) Comparable numbers of cleaved caspase-3-stained cells were seen in WT and mutant umbilical cords (n = 3 cords for each group. Error bars represent SD; p values determined by Student's t test).

(F) $Adamts9^{Gt/Gt}$ umbilical vessels show significantly smaller luminal areas than WT vessels (n = 5 cords for each group. Error bars represent SEM; p values are determined by Student's t test).

(G–J) Immunostaining for versican (GAGβ) demonstrates versican in both WT and $Adamts9^{Gt/Gt}$ umbilical vessels (G and H), but cleaved versican (anti-DPEAAE) is present only in WT umbilical cord.

(K and L) HAbp staining was comparable in WT and mutant cords.

(M–P) Fibronectin (M and N) and fibrillin-2 (O and P) immunostaining demonstrated stronger staining in $Adamts9^{Gt/Gt}$ umbilical vessels.

(Q and R) Elastin immunostaining showed a non-laminar staining pattern in WT umbilical vessels and weaker staining in the mutant.

(S and T) Collagen-IV antibody comparably stained WT and $Adamts9^{Gt/Gt}$ umbilical cords.

(U–X) Phalloidin (U and V) and phosphorylated MLC staining (W and X) demonstrated an attenuated cytoskeletal network and suggested reduced contractility in the $Adamts9^{Gt/Gt}$ VSMCs. Boxed areas are illustrated at higher magnification in (G')–(V').

A, artery; V, vein; En, endothelium. Scale bars represent 100 μm in (A), (C), and (G)–(V); 25 μm in (W) and (X); and 5 μm in (B). See also Figure S4.
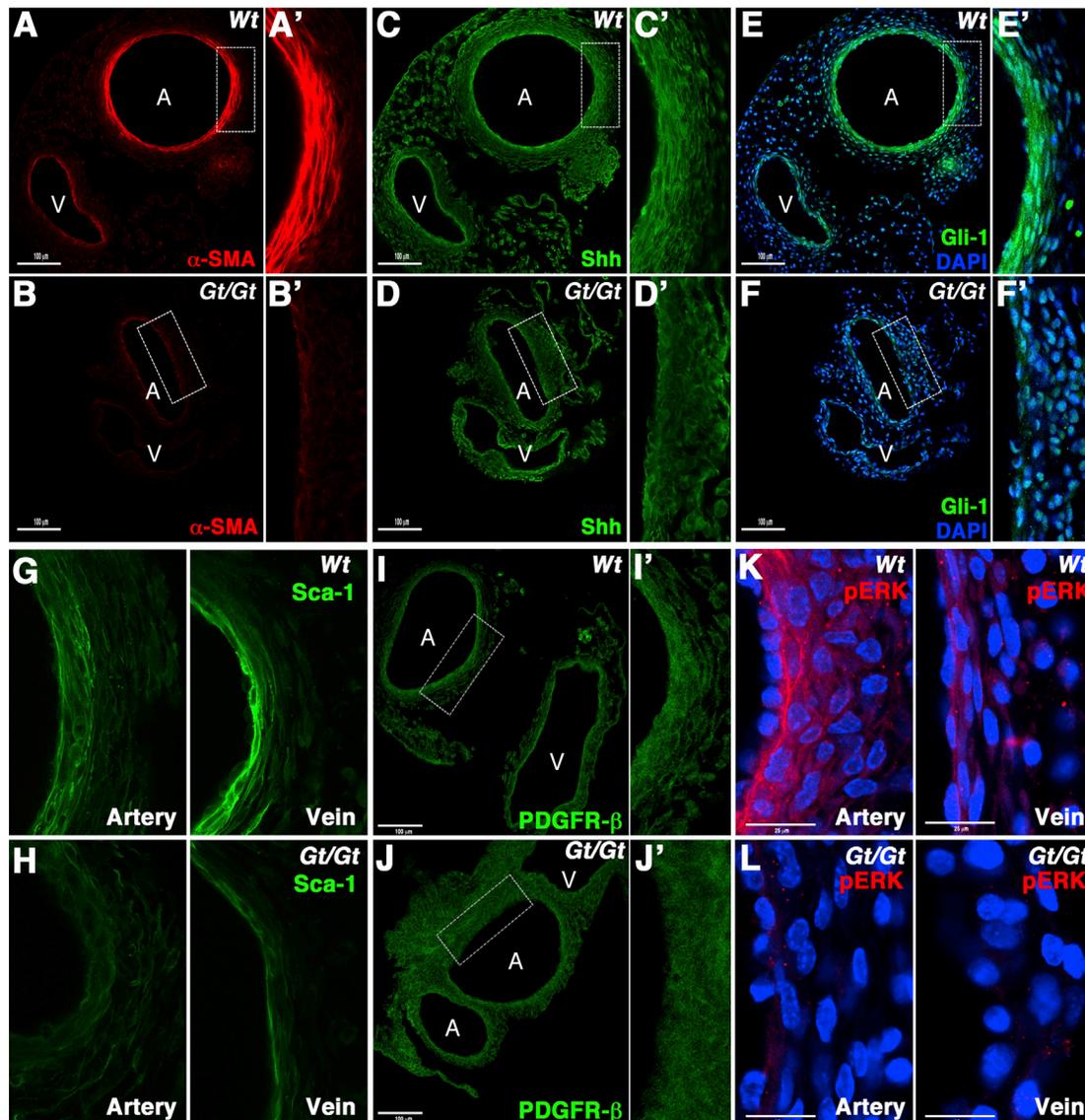
Figure 3. Dysregulated Shh and PDGF-B Signaling in *Adamts9^{Gt/Gt}* Umbilical Cords

(A–B') Strong α-SMA staining of VSMCs in E12.5 WT, but not *Adamts9^{Gt/Gt}*, umbilical vessels. Magnified images of the arterial wall are illustrated in (A') and (B').

(C–F') Shh (C and D) and Gli-1 (E and F) immunostaining was weaker in the *Adamts9^{Gt/Gt}* umbilical vessels. Boxed areas are illustrated at higher magnification in (C')–(F').

(G and H) Sca-1 is localized to the innermost VSMC layer in the WT umbilical artery and vein, but has reduced intensity in the mutant.

(I–L) Immunostaining for PDGFRβ (I–J) and pERK1/2 (K and L) in WT and mutant umbilical cords shows weak staining for PDGFRβ and no staining for pERK1/2 in the mutant. The boxed areas are illustrated at higher magnification in (I') and (J'). Scale bars represent 100 μm in (A)–(J) and 25 μm in (K) and (L).

Pdgfb^{−/−} embryos have short umbilical cords (Hellström et al., 1999). PDGFR-β signaling activates Shh during vascular maturation (Yao et al., 2014) and was implicated in radial growth and SMC reorientation during pulmonary arterial wall development (Greif et al., 2012). PDGF-B, the ligand for PDGFRβ, is produced by vascular endothelial cells and contains a C-terminal ECM retention motif (Andrae et al., 2008), which interacts with heparan-sulfate proteoglycans. We observed strong PDGFRβ expression in juxta-endothelial VSMCs in WT umbilical vessels, whereas mutant umbilical vessels showed reduced expression

(Figures 3I–3J'). Phosphorylated-ERK1/2 staining, reporting PDGFR-β signaling, among other pathways, revealed a lack of activation of the extracellular signal-regulated kinase/mitogen-activated protein kinase (ERK/MAPK) pathway in mutant VSMCs (Figures 3K and 3L). Since the ERK/MAPK pathway is a major regulator of cytoskeletal dynamics in many cell types (Kolch, 2005), this may explain the reduced actin cytoskeleton and impaired orthogonal rotation in the mutant VSMCs. Thus, two major pathways regulating VSMC recruitment and differentiation, i.e., Shh and PDGFR-β pathways, are active during normal

umbilical cord development and compromised in *Adamts9*[Gt/Gt] cords.

The Preferred Radial Orientation of Cilia Is Disrupted in *Adamts9*[Gt/Gt] Umbilical Cord Mesenchyme

Primary cilia are cellular organelles projecting into the microenvironment that are implicated in Shh, PDGFRα, and Wnt signaling (Fliegauf et al., 2007). They may work as ECM sensors in connective tissues (Donnelly et al., 2008; McGlashan et al., 2006) since ECM molecules such as collagens and proteoglycans interact with the cilium membrane (Jensen et al., 2004). Integrins α3, α5, and β1 localize to the primary cilium of aortic VSMCs and were implicated in fibronectin-induced Ca^{+2} signaling (Lu et al., 2008; McGlashan et al., 2006; Praetorius et al., 2004). Confocal Z-stack projections of WT umbilical cords stained with acetylated tubulin revealed primary cilia in most mesenchymal and mesothelial cells, but not vascular endothelium (Figures 4A–4D). Most umbilical VSMCs lacked primary cilia (Figure 4A), contrasting with cilia reported in adult mouse aortic VSMCs (Lu et al., 2008). Primary cilia in the adventitium and Wharton's jelly of WT umbilical cords had a preferred radial orientation, whereas *Adamts9*[Gt/Gt] umbilical cords had a high percentage of cells whose cilia veered away from this orientation (arrowheads in Figures 4A' and 4B'). Radar plots of the minor angle of individual cilia to a radial vector showed that WT cells had an average cilia angle of 36.95 degrees, while mutant cells had an average angle of 56.08 degrees (Figure 4E). Integrins β1 and α5 co-localized with some umbilical cord mesenchymal cilia (Figure 4F), supporting a cilium-ECM interaction. Thus, altered ECM dynamics in the mutant umbilical cord is not only accompanied by compromised Shh signaling, but altered orientation of the primary cilium, a key participant in the pathway (Goetz and Anderson, 2010).

Tbx4-Cre-Mediated Conditional Deletion of *Adamts9*, but not VSMC-Specific Deletion, Recapitulates the *Adamts9*[Gt/Gt] Defect

Conditional deletion of *Adamts9* using *Tbx4*-Cre, which is expressed in the developing hind limbs, lung mesenchyme, and the umbilical cord mesenchyme, but not in the embryonic heart or yolk sac, (Greif et al., 2012; Naiche et al., 2011) led to significantly shorter umbilical cords than *Adamts9*[Fl/+] and *Tbx4*-Cre; *Adamts9*[Fl/+] siblings by E12.5 (Figures S5A–S5C). A dual tomato reporter showed that *Tbx4*-Cre expression overlapped substantially with *Adamts9* in the adventitia (Figures S5D–S5G) but not Wharton's jelly mesenchyme or vascular endothelium (Figures S5E and S5F). Impairment of VSMC rotation in *Tbx4*-Cre conditionally deleted umbilical cords was seen, but was less severe than in *Adamts9*[Gt/Gt] umbilical cords (Figures S5H–S5M), consistent with spatially limited deletion by *Tbx4*-Cre, and did not impair embryo survival. Conditional deletion by *Tagln*-Cre did not impair embryonic survival or umbilical cord growth (Figures S5N–S5P) since deletion occurred only in VSMC, but not most cells expressing ADAMTS9 (Figures S5Q–S5S), and had no impact on VSMC rotation (Figures S5T–S5Y). Thus, ADAMTS9 secreted by adventitial cells and mesenchyme influences VSMCs non-autonomously during umbilical vessel development.

A Proposed Role for ADAMTS9-Mediated ECM Dynamics in Umbilical Cord VSMC Differentiation

We show that the murine umbilical cord undergoes rapid growth, along with longitudinal and radial growth of umbilical vessels after 11.5 days of gestation. Umbilical arteries acquire three to four layers of VSMC by E14.5, with one to two layers constituting the corresponding venous wall. Around E12.5, after commitment to the SMC lineage and acquisition of SMA expression, the VSMCs reorient orthogonally (i.e., rotate), proliferate, and begin to build a vascular matrix containing elastin. Wharton's jelly mesenchyme remains undifferentiated throughout and contains abundant ECM. Between Wharton's jelly and VSMCs, a de facto adventitia comprising closely packed, longitudinally oriented cells is formed. Primary cilia, found here, and in the mesenchymal and mesothelial cells of the umbilical cord are normally radially oriented. This umbilical cord vasculature organization (Figure 5A) appears to be maintained through further development.

Upon secretion, ADAMTS9 localizes to the cell surface, presumably binding to pericellular matrix or cell-surface proteins, where it is processed by furin, but it is also released from cells and detectable in their medium (Koo et al., 2006, 2007). Unimpaired normal gastrulation in *Adamts9*[Gt/Gt] embryos, yet impeded later development (including cooperative functions with *Adamts20*), suggests existence of two functional pools of ADAMTS9 (Figure 5B). The cell-proximate pool, i.e., pericellular ADAMTS9, albeit at lower levels in ADAMTS9-GT, suffices where ECM resides close to the cell surface (such as in the gastrulating embryo). In contrast, the secreted or "cell-distal" pool, shown to be lacking in ADAMTS9-GT-transfected cells, acts at longer range and non-cell-autonomously and is crucial where interstitial ECM is abundant (Figure 5B). We propose that long-range ADAMTS9 activity becomes increasingly necessary with enhanced interstitial ECM as embryogenesis progresses.

We show that VSMC specialization, including orthogonal reorientation, requires proper ECM dynamics mediated by ADAMTS9 acting non-autonomously in the umbilical cord. Mechanistically, ECM interactions of Shh and PDGF-BB are critical for their normal function (Stenzel et al., 2009; Varjosalo and Taipale, 2008) and could be impaired by altered ECM dynamics, which may affect their release or transport. Altered ECM composition and density could also affect cilium orientation, as shown here, and directly impair Shh signaling (Figure 5B). We propose that activation of the MAPK/ERK pathway in VSMCs in response to PDGFR-β and other signaling inputs may regulate cytoskeletal dynamics required for VSMC reorientation (Figure 5B). Indeed, in *Adamts9*[Gt/Gt] umbilical cords, F-actin, smooth muscle α-actin, and phosphorylated myosin light chain (MLC) staining were dramatically reduced, and the final effect of the altered ECM dynamics would be to compromise cell rotation through these cytoskeletal changes potentially coupled with impedance by enhanced pericellular matrix.

EXPERIMENTAL PROCEDURES

Transgenic Mice and Genotyping

R1 male embryonic stem cells with insertion of UPATrap at the *Adamts9* locus were injected into blastocysts and chimeras were bred to WT
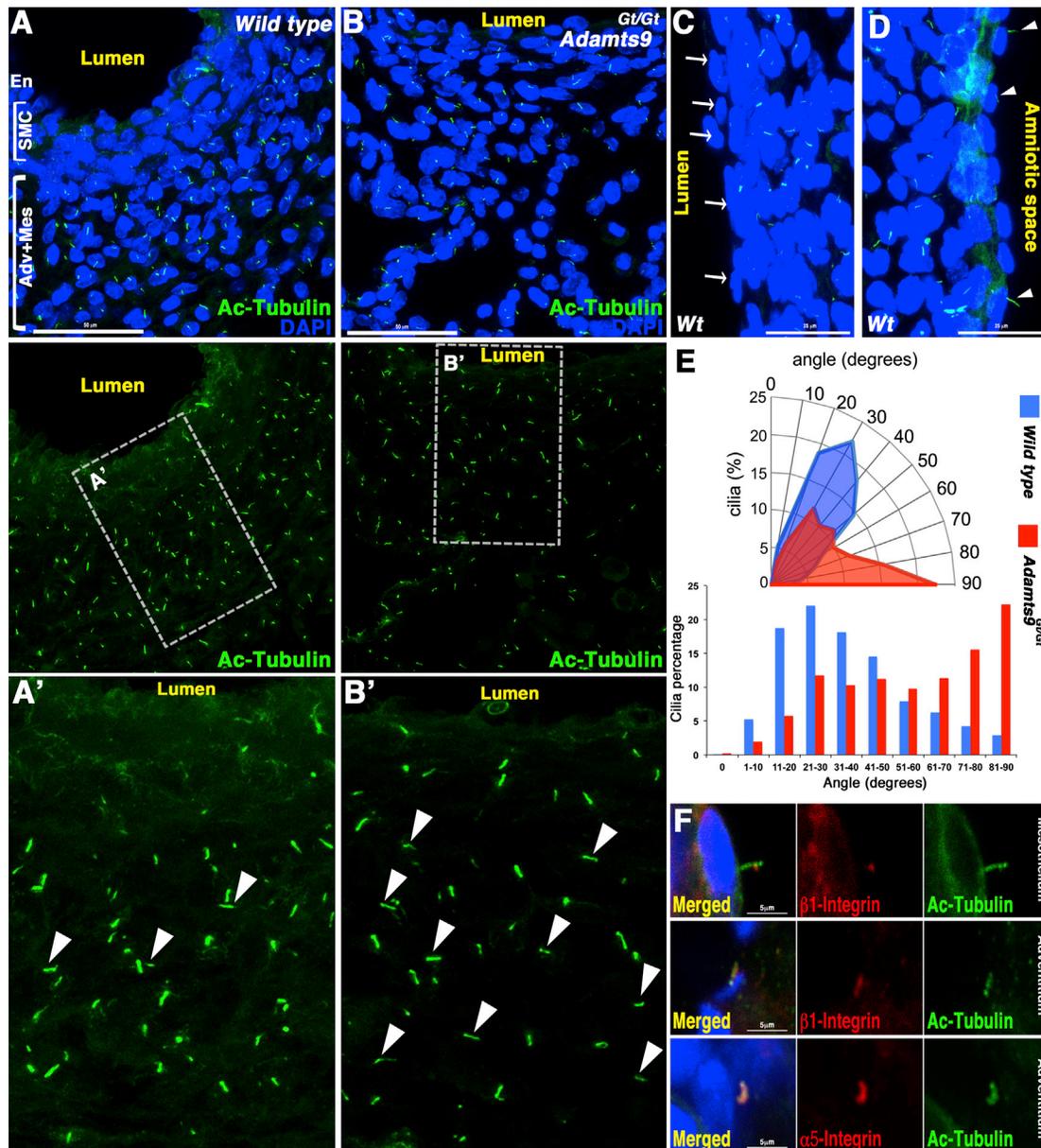
Figure 4. Primary Cilium Orientation Is Perturbed in *Adamts9^{Gt/Gt}* Umbilical Cords

(A–D) Maximum intensity projections of confocal Z sections from the arterial wall of E12.5 WT (A and A') and *Adamts9^{Gt/Gt}* (B and B') umbilical cords stained with acetylated tubulin (green) and DAPI (blue). Note paucity of cilia in WT VSMC and high prevalence in mesenchyme. Arrowheads in (A') and (B') point to cilia oriented orthogonal to a radial vector in the *Adamts9^{Gt/Gt}* vessels with fewer seen in WT. (C and D) Primary cilia are absent in vascular endothelium (C, arrows) but are present in the mesothelium (D, arrowheads).

(E) Measurement of minor angle of the cilium to a radial vector arising from the lumen of WT and mutant umbilical vessels, binned in 10-degree intervals (n = 4 cords for each group). The radar plot demonstrates that a high percentage of mutant cilia are misaligned.

(F) Co-immunostaining for acetylated tubulin (green) and integrins β1 and α5 (red) in WT umbilical cords shows that in some mesenchymal cells, integrins localized to cilia.

Scale bars represent 50 μm in (A) and (B), 25 μm in (C) and (D), and 5 μm in (F).

mice for germline transmission of the trapped allele. *Adamts9^{LacZ/+}* (Kern et al., 2010), and the *Adamts20* mutant *Adamts20^{bt-Bei1}* (referred to as *Adamts20^{Bt}*) (Rao et al., 2003; Silver et al., 2008) were described previously. Germline deletion of *Adamts9^{fl}* (RRID:JAX_026103) provided the *Adamts9^{Del}* allele (Dubail et al., 2014). *Adamts^{fl}* mice were crossed extensively with *ROSA^{mT/mG}* reporter mice (Muzumdar et al., 2007) to achieve

linkage of the two transgenes on chr 6. *Tbx4*-Cre (Naiche et al., 2011) and *Tagln*-Cre (Holtwick et al., 2002) strains were used for *Adamts9^{fl}* conditional deletion. Additional details are provided in Supplemental Experimental Procedures. The mouse work was conducted at the Biological Resources Unit of the Cleveland Clinic under protocols approved by the Institutional Animal Care and Use Committee. Mouse tissues were
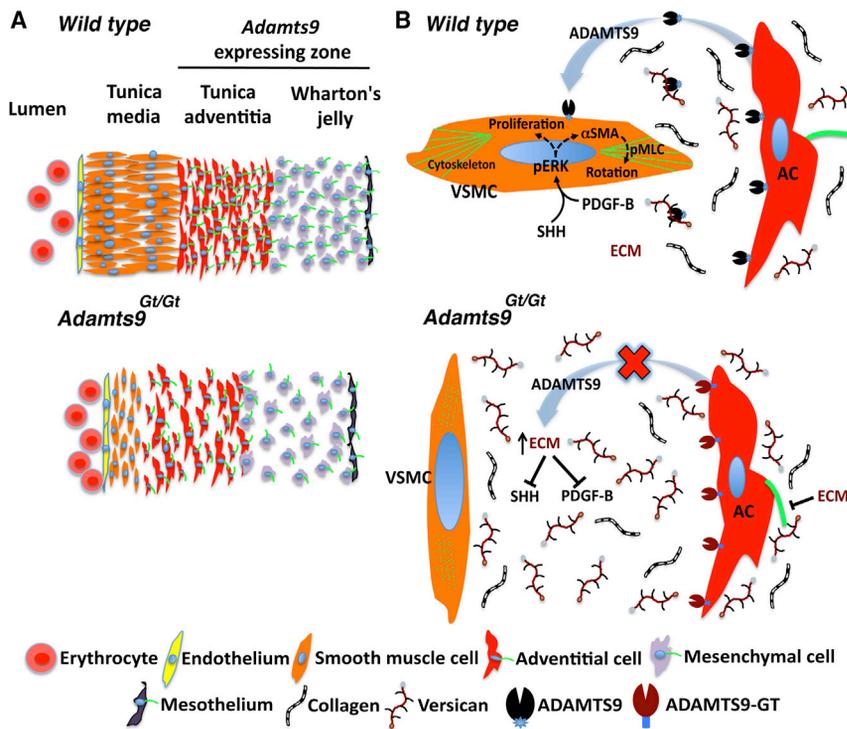
Figure 5. ADAMTS9-Mediated ECM Dynamics Regulates VSMC Development in the Umbilical Cord

(A) The normal umbilical vessel has three major layers. VSMCs are oriented orthogonal to adventitial cells, and primary cilia (green) have a preferred radial orientation, which is perturbed in the mutant.

(B) Two pools of ADAMTS9, pericellular and secreted (black) in adventitial and mesenchymal cells, cleave versican to facilitate ECM remodeling and enable normal Shh and PDGF-B signaling via ERK1/2 phosphorylation, which regulates VSMC differentiation. In $Adamts9^{Gt/Gt}$ ADAMTS9-GT (brown) is cell-surface restricted, and versican turnover is reduced. Altered ECM dynamics may affect release and transport of Shh and PDGF-B or act via ECM sensing by the cilium. Failed orthogonal rotation may result from reduced MAPK/ERK activation, an effete cytoskeleton, loss of p-MLC and αSMA, or physical impedance by accumulated pericellular ECM around $Adamts9^{Gt/Gt}$ VSMCs.

See also Figure S5.

obtained after euthanasia, performed as recommended by the American Veterinary Association Panel on Euthanasia.

Embryo Analysis

Paraformaldehyde-fixed tissue was embedded in ultrapure agarose and vibratome-sectioned or embedded in paraffin for sectioning. Analysis of sections by immunofluorescence or fluorescence microscopy, ascertainment of primary cilium orientation, and TEM is described in Supplemental Experimental Procedures.

Molecular Cloning, Cell and Biochemical Analysis

Determination of the UPATrap insertion site, generation of plasmids expressing truncated ADAMTS9, molecular cloning of ADAMTS9 splice variants, cell culture, transfection, biotinylation, and western blotting is described in Supplemental Experimental Procedures.

SUPPLEMENTAL INFORMATION

Supplemental Information includes Supplemental Experimental Procedures, five figures, and one table and can be found with this article online at http://dx.doi.org/10.1016/j.celrep.2015.05.005.

AUTHOR CONTRIBUTIONS

S.N. designed and conducted experiments and wrote the manuscript. C.M.N. conducted experiments. S.S.A. designed experiments and wrote the manuscript.

REFERENCES

Andrae, J., Gallini, R., and Betsholtz, C. (2008). Role of platelet-derived growth factors in physiology and medicine. Genes Dev. 22, 1276–1312.

Apte, S.S. (2009). A disintegrin-like and metalloprotease (reprolysin-type) with thrombospondin type 1 motif (ADAMTS) superfamily: functions and mechanisms. J. Biol. Chem. 284, 31493–31497.

Armulik, A., Genové, G., and Betsholtz, C. (2011). Pericytes: developmental, physiological, and pathological perspectives, problems, and promises. Dev. Cell 21, 193–215.

Benirschke, K., Burton, G.J., and Baergen, R.N., eds. (2012). Anatomy and pathology of the umbilical cord. In Pathology of the Human Placenta (Berlin Heidelberg: Springer-Verlag), pp. 309–376.

Blelloch, R., Anna-Arriola, S.S., Gao, D., Li, Y., Hodgkin, J., and Kimble, J. (1999). The gon-1 gene is required for gonadal morphogenesis in Caenorhabditis elegans. Dev. Biol. 216, 382–393.

Bonnans, C., Chou, J., and Werb, Z. (2014). Remodelling the extracellular matrix in development and disease. Nat. Rev. Mol. Cell Biol. 15, 786–801.

Camenisch, T.D., Spicer, A.P., Brehm-Gibson, T., Biesterfeldt, J., Augustine, M.L., Calabro, A., Jr., Kubalak, S., Klewer, S.E., and McDonald, J.A. (2000). Disruption of hyaluronan synthase-2 abrogates normal cardiac morphogenesis and hyaluronan-mediated transformation of epithelium to mesenchyme. J. Clin. Invest. 106, 349–360.

Donnelly, E., Williams, R., and Farnum, C. (2008). The primary cilium of connective tissue cells: imaging by multiphoton microscopy. Anat. Rec. (Hoboken) 291, 1062–1073.

Dubail, J., Aramaki-Hattori, N., Bader, H.L., Nelson, C.M., Katebi, N., Matuska, B., Olsen, B.R., and Apte, S.S. (2014). A new Adamts9 conditional mouse allele

OPEN
ACCESS
CellPress

identifies its non-redundant role in interdigital web regression. Genesis *52*, 702–712.

Dupuis, L.E., McCulloch, D.R., McGarity, J.D., Bahan, A., Wessels, A., Weber, D., Diminich, A.M., Nelson, C.M., Apte, S.S., and Kern, C.B. (2011). Altered versican cleavage in ADAMTS5 deficient mice; a novel etiology of myxomatous valve disease. Dev. Biol. *357*, 152–164.

Enomoto, H., Nelson, C.M., Somerville, R.P.T., Mielke, K., Dixon, L.J., Powell, K., and Apte, S.S. (2010). Cooperation of two ADAMTS metalloproteases in closure of the mouse palate identifies a requirement for versican proteolysis in regulating palatal mesenchyme proliferation. Development *137*, 4029–4038.

Fliegauf, M., Benzing, T., and Omran, H. (2007). When cilia go bad: cilia defects and ciliopathies. Nat. Rev. Mol. Cell Biol. *8*, 880–893.

Goetz, S.C., and Anderson, K.V. (2010). The primary cilium: a signalling centre during vertebrate development. Nat. Rev. Genet. *11*, 331–344.

Gogiel, T., Bańkowski, E., and Jaworski, S. (2003). Proteoglycans of Wharton's jelly. Int. J. Biochem. Cell Biol. *35*, 1461–1469.

Greif, D.M., Kumar, M., Lighthouse, J.K., Hum, J., An, A., Ding, L., Red-Horse, K., Espinoza, F.H., Olson, L., Offermanns, S., and Krasnow, M.A. (2012). Radial construction of an arterial wall. Dev. Cell *23*, 482–493.

Haraguchi, R., Motoyama, J., Sasaki, H., Satoh, Y., Miyagawa, S., Nakagata, N., Moon, A., and Yamada, G. (2007). Molecular analysis of coordinated bladder and urogenital organ formation by Hedgehog signaling. Development *134*, 525–533.

Hellström, M., Kalén, M., Lindahl, P., Abramsson, A., and Betsholtz, C. (1999). Role of PDGF-B and PDGFR-beta in recruitment of vascular smooth muscle cells and pericytes during embryonic blood vessel formation in the mouse. Development *126*, 3047–3055.

Holtwick, R., Gotthardt, M., Skryabin, B., Steinmetz, M., Potthast, R., Zetsche, B., Hammer, R.E., Herz, J., and Kuhn, M. (2002). Smooth muscle-selective deletion of guanylyl cyclase-A prevents the acute but not chronic effects of ANP on blood pressure. Proc. Natl. Acad. Sci. USA *99*, 7142–7147.

Ismat, A., Cheshire, A.M., and Andrew, D.J. (2013). The secreted AdamTS-A metalloprotease is required for collective cell migration. Development *140*, 1981–1993.

Jensen, C.G., Poole, C.A., McGlashan, S.R., Marko, M., Issa, Z.I., Vujcich, K.V., and Bowser, S.S. (2004). Ultrastructural, tomographic and confocal imaging of the chondrocyte primary cilium in situ. Cell Biol. Int. *28*, 101–110.

Kern, C.B., Wessels, A., McGarity, J., Dixon, L.J., Alston, E., Argraves, W.S., Geeting, D., Nelson, C.M., Menick, D.R., and Apte, S.S. (2010). Reduced versican cleavage due to Adamts9 haploinsufficiency is associated with cardiac and aortic anomalies. Matrix Biol. *29*, 304–316.

Kolch, W. (2005). Coordinating ERK/MAPK signalling through scaffolds and inhibitors. Nat. Rev. Mol. Cell Biol. *6*, 827–837.

Koo, B.H., Longpré, J.M., Somerville, R.P., Alexander, J.P., Leduc, R., and Apte, S.S. (2006). Cell-surface processing of pro-ADAMTS9 by furin. J. Biol. Chem. *281*, 12485–12494.

Koo, B.H., Longpré, J.M., Somerville, R.P., Alexander, J.P., Leduc, R., and Apte, S.S. (2007). Regulation of ADAMTS9 secretion and enzymatic activity by its propeptide. J. Biol. Chem. *282*, 16146–16154.

Koo, B.H., Coe, D.M., Dixon, L.J., Somerville, R.P., Nelson, C.M., Wang, L.W., Young, M.E., Lindner, D.J., and Apte, S.S. (2010). ADAMTS9 is a cell-autonomously acting, anti-angiogenic metalloprotease expressed by microvascular endothelial cells. Am J Pathol. *176*, 1494–1504.

Kwon, G.S., Viotti, M., and Hadjantonakis, A.K. (2008). The endoderm of the mouse embryo arises by dynamic widespread intercalation of embryonic and extraembryonic lineages. Dev. Cell *15*, 509–520.

Lu, C.J., Du, H., Wu, J., Jansen, D.A., Jordan, K.L., Xu, N., Sieck, G.C., and Qian, Q. (2008). Non-random distribution and sensory functions of primary cilia in vascular smooth muscle cells. Kidney Blood Press. Res. *31*, 171–184.

McCulloch, D.R., Nelson, C.M., Dixon, L.J., Silver, D.L., Wylie, J.D., Lindner, V., Sasaki, T., Cooley, M.A., Argraves, W.S., and Apte, S.S. (2009). ADAMTS metalloproteases generate active versican fragments that regulate interdigital web regression. Dev. Cell *17*, 687–698.

McGlashan, S.R., Jensen, C.G., and Poole, C.A. (2006). Localization of extracellular matrix receptors on the chondrocyte primary cilium. J. Histochem. Cytochem. *54*, 1005–1014.

Miner, J.H., Li, C., Mudd, J.L., Go, G., and Sutherland, A.E. (2004). Compositional and structural requirements for laminin and basement membranes during mouse embryo implantation and gastrulation. Development *131*, 2247–2256.

Mouw, J.K., Ou, G., and Weaver, V.M. (2014). Extracellular matrix assembly: a multiscale deconstruction. Nat. Rev. Mol. Cell Biol. *15*, 771–785.

Muzumdar, M.D., Tasic, B., Miyamichi, K., Li, L., and Luo, L. (2007). A global double-fluorescent Cre reporter mouse. Genesis *45*, 593–605.

Naiche, L.A., Arora, R., Kania, A., Lewandoski, M., and Papaioannou, V.E. (2011). Identity and fate of Tbx4-expressing cells reveal developmental cell fate decisions in the allantois, limb, and external genitalia. Dev. Dyn. *240*, 2290–2300.

Nandadasa, S., Tao, Q., Menon, N.R., Heasman, J., and Wylie, C. (2009). N- and E-cadherins in Xenopus are specifically required in the neural and non-neural ectoderm, respectively, for F-actin assembly and morphogenetic movements. Development *136*, 1327–1338.

Naso, M.F., Morgan, J.L., Buchberg, A.M., Siracusa, L.D., and Iozzo, R.V. (1995). Expression pattern and mapping of the murine versican gene (Cspg2) to chromosome 13. Genomics *29*, 297–300.

Passman, J.N., Dong, X.R., Wu, S.P., Maguire, C.T., Hogan, K.A., Bautch, V.L., and Majesky, M.W. (2008). A sonic hedgehog signaling domain in the arterial adventitia supports resident Sca1+ smooth muscle progenitor cells. Proc. Natl. Acad. Sci. USA *105*, 9349–9354.

Peters, J.H., and Hynes, R.O. (1996). Fibronectin isoform distribution in the mouse. I. The alternatively spliced EIIIB, EIIIA, and V segments show widespread codistribution in the developing mouse embryo. Cell Adhes. Commun. *4*, 103–125.

Praetorius, H.A., Praetorius, J., Nielsen, S., Frokiaer, J., and Spring, K.R. (2004). Beta1-integrins in the primary cilium of MDCK cells potentiate fibronectin-induced Ca2+ signaling. Am. J. Physiol. Renal Physiol. *287*, F969–F978.

Rao, C., Foernzler, D., Loftus, S.K., Liu, S., McPherson, J.D., Jungers, K.A., Apte, S.S., Pavan, W.J., and Beier, D.R. (2003). A defect in a novel ADAMTS family member is the cause of the belted white-spotting mutation. Development *130*, 4665–4672.

Sandy, J.D., Westling, J., Kenagy, R.D., Iruela-Arispe, M.L., Verscharen, C., Rodriguez-Mazaneque, J.C., Zimmermann, D.R., Lemire, J.M., Fischer, J.W., Wight, T.N., and Clowes, A.W. (2001). Versican V1 proteolysis in human aorta in vivo occurs at the Glu441-Ala442 bond, a site that is cleaved by recombinant ADAMTS-1 and ADAMTS-4. J. Biol. Chem. *276*, 13372–13378.

Silver, D.L., Hou, L., Somerville, R., Young, M.E., Apte, S.S., and Pavan, W.J. (2008). The secreted metalloprotease ADAMTS20 is required for melanoblast survival. PLoS Genet. *4*, e1000003.

Sobolewski, K., Bańkowski, E., Chyczewski, L., and Jaworski, S. (1997). Collagen and glycosaminoglycans of Wharton's jelly. Biol. Neonate *71*, 11–21.

Stankunas, K., Hang, C.T., Tsun, Z.Y., Chen, H., Lee, N.V., Wu, J.I., Shang, C., Bayle, J.H., Shou, W., Iruela-Arispe, M.L., and Chang, C.P. (2008). Endocardial Brg1 represses ADAMTS1 to maintain the microenvironment for myocardial morphogenesis. Dev. Cell *14*, 298–311.

Stenzel, D., Nye, E., Nisancioglu, M., Adams, R.H., Yamaguchi, Y., and Gerhardt, H. (2009). Peripheral mural cell recruitment requires cell-autonomous heparan sulfate. Blood *114*, 915–924.

Stupka, N., Kintakas, C., White, J.D., Fraser, F.W., Hanciu, M., Aramaki-Hattori, N., Martin, S., Coles, C., Collier, F., Ward, A.C., et al. (2013). Versican processing by a disintegrin-like and metalloproteinase domain with thrombospondin-1 repeats proteinases-5 and -15 facilitates myoblast fusion. J. Biol. Chem. *288*, 1907–1917.

Varjosalo, M., and Taipale, J. (2008). Hedgehog: functions and mechanisms. Genes Dev. *22*, 2454–2472.

Wagenseil, J.E., and Mecham, R.P. (2009). Vascular extracellular matrix and arterial mechanics. Physiol. Rev. *89*, 957–989.

Yao, Q., Renault, M.A., Chapouly, C., Vanderdonck, S., Belloc, I., Jaspard-Vinassa, B., Daniel-Lamazière, J.M., Laffargue, M., Merched, A., Desgranges, C., and Gadeau, A.P. (2014). Sonic hedgehog mediates a novel pathway of PDGF-BB-dependent vessel maturation. Blood *123*, 2429–2437.